International Journal of Control, Automation and Systems 18(3) (2020) 575-586
http://dx.doi.org/10.1007/s12555-019-0548-9
ISSN:1598-6446 eISSN:2005-4092
http://www.springer.com/12555

Analysis of Electromagnetic Waves Attenuation for Underwater Localization in Structured Environments

Daegil Park, Wan Kyun Chung, and Jinhyun Kim*

Abstract: Range sensors based on electromagnetic (EM) waves attenuation along the target distance yield precise distance estimation with a high resolution, depending on the distance. However, their application in a structured underwater environment is difficult because the characteristics of EM waves attenuation in such environments are not considered. In this study, characteristics of EM waves propagation and signal interference effects due to structures are analyzed, and an EM waves distance-attenuation model for a structured underwater environment is proposed, along with sensor installation guidelines. The characteristics of EM waves propagation and the proposed sensor model are verified by several experiments, and the proposed sensor model yields greater accuracy positioning results compared to the previous model.

Keywords: Electromagnetic waves, localization, marine robot, range sensor, underwater positioning.

1. INTRODUCTION

Construction of underwater infrastructure for the use of offshore plants and wind power stations is expanding; thus, many studies have recently been conducted regarding the use of unmanned underwater vehicles (UUVs) to maintain such structures. In particular, many investigations of underwater localization have been performed, as this localization is essential for UUV perception in an underwater environment [1–3]. Acoustic sensors are conventionally used for underwater localization, as a sonar sensor has a long range and exhibits reliable operation in underwater environments. However, sonar performance in complex structured environments is not guaranteed because of the multi-path effect, diffraction, and scattering. Moreover, the number of underwater structures is increasing, and many applications therefore require precise position estimation capability when employed in complex structured environments such as offshore plants and docking structures [4–10]. Therefore, an alternative sensor for use in underwater structured environments is required.

To overcome the aforementioned issues, we previously suggested a position estimation method that exploits the characteristics of electromagnetic (EM) waves attenuation along the target distance. The proposed sensor presented an extremely precise distance estimation with high resolution, depending on the distance. EM waves propagation is considerably faster than sound wave propagation. Therefore, use of EM waves can yield a high sampling rate; this characteristic can be exploited for dynamic object tracking [11–14].

However, it is difficult to utilize the proposed localization system in real-time applications because the characteristics of EM waves attenuation in a structured underwater environment are neglected. In previous studies, only the received signal strengths (RSSs) of EM waves in a lossy medium were considered, with the accuracy verified under ideal conditions [11, 15–17]. However, most underwater positioning applications and sensor installation conditions pertain to complex and structured environments as shown in Fig. 1. Therefore, analysis of EM waves propagation near various objects is necessary to facilitate use of EM waves attenuation sensors in structured environments.

In this paper, the characteristics of EM waves propagation, and signal interference effects of structures are analyzed. The Fresnel zone and near field are taken as the distortion criteria, and various interferences in the water medium are verified through feasibility tests. Based on

Manuscript received July 18, 2019; revised November 15, 2019; accepted December 13, 2019. Recommended by Associate Editor Son-Cheol Yu under the direction of Editor-in-Chief Keum-Shik Hong. This research was supported by Institute of Civil Military Technology Cooperation (ICMTC) of Agency for Defense Development (ADD), funded by Defense Acuisition Program Administration (DAPA) and Ministry of Trade, Industry and Energy (MOTIE) (Developement of multi-sensor fusion based AUVs terminal guidance and docking technology, 17-CM- RB-16), Korea.

Daegil Park is with the Marine Robotics R&D Division, Korea Institute of Robot and Technology Convergence, 39 Jigok-ro, Nam-gu, Pohang 37666, Korea (e-mail: daegilpark@kiro.re.kr). Wan Kyun Chung is with the Department of Mechanical Engineering, Pohang University of Science and Technology (POSTECH), 77 Cheongam-ro, Nam-gu, Pohang 37673, Korea (e-mail: wkchung@postech.ac.kr). Jinhyun Kim is with the Department of Mechanical & Automotive Engineering, Seoul National University of Science and Technology (SeoulTECH), 232 Gongneung-ro, Nowon-gu, Seoul 01811, Korea (e-mail: jinhyun@seoultech.ac.kr).
* Corresponding author.

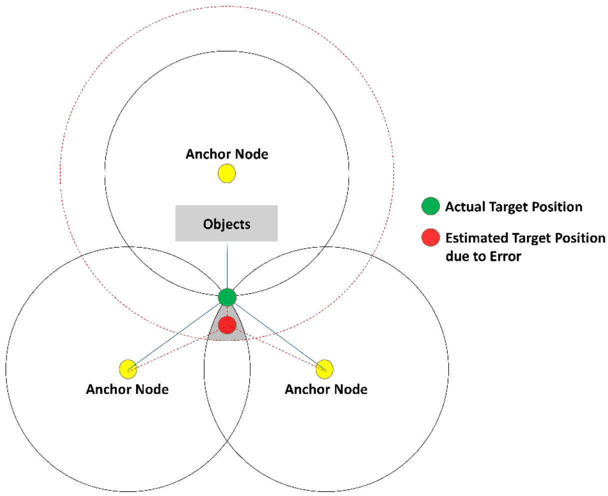

Fig. 1. Conceptual diagram of biased localization result caused by structure. The structure induces additional EM waves attenuation and functions as an additional gap between nodes.

these analyses and experiments, an EM waves distance-attenuation model for a structured underwater environment is suggested, along with sensor installation guidelines.

The remainder of this paper is organized as follows: Section 2 introduces previous work regarding underwater range sensor models for ideal conditions, along with the model parameter estimation scheme for an infrastructure-based localization system. A theoretical analysis of EM waves interference near objects is presented in Section 3. Verification of the underwater characteristics of EM waves propagation through several experiments is reported in Section 4. The signal loss due to object penetration is considered as the attenuation model for structured environments in Section 5. Section 6 reports the proposed sensor model performance, based on comparison of the estimated sensor parameters and 2D localization in the structured environment. Finally, Section 7 presents a summary, conclusion, and outline for future work.

2. DERIVATION OF UNDERWATER SENSOR MODEL AND MODEL PARAMETER ESTIMATION

2.1. Underwater range sensor model

EM waves attenuation according to distance is affected by the antenna shape, frequency, and medium properties. In air, the attenuation is relatively small to be neglected. Therefore, we can consider the energy diffusion as a function of distance using the Friis-Shelkunoff formula [18]. However, in other media with larger attenuation, such as water or oil, the Friis-Shelkunoff formula is insufficient for the distance calculation. In that case, an additional formula that accounts for the medium properties (e.g., attenuation and absorption) is needed. Therefore, we previously proposed a novel underwater sensor model combining both, energy diffusion and energy absorption by the medium [11, 17].

2.1.1 Friis-Shelkunoff formula

The Friis-Shelkunoff formula is a basic antenna theory that calculates the separation distance R between a transmission antenna with gain G_T, and a receiving antenna with gain G_R, for EM waves with frequency f. As a result of the low attenuation of EM waves in air, the attenuation is assumed to be zero.

If the antennas are aligned and R exceeds the near field distance ($R_n = \frac{L^2}{\lambda}$, where L is the maximum dimension of the distance), the relationship between the received signal power P_R and R is given by the Friis-Shelkunoff formula:

$$P_R = \frac{P_T G_T G_R \lambda^2}{(4\pi R)^2} \text{ [mW]}, \tag{1}$$

where P_T is the transmitted signal power and λ is the wavelength of the EM waves.

2.1.2 Attenuation constant

Generally, the power attenuation induced by the medium as a function of distance can be expressed by the attenuation constant of the plane waves equation [19], where P_R is defined by P_T, R, and the attenuation coefficient α as

$$P_R = P_T e^{-2\alpha R} \text{ [mW]}, \tag{2}$$

where α is the real part of the propagation constant γ, and is given by

$$\alpha = \omega\sqrt{\varepsilon\mu}\sqrt{\frac{1}{2}\left[\sqrt{1+\frac{\sigma^2}{\omega^2\varepsilon^2}}-1\right]}, \tag{3}$$

where ε and μ are the permittivity and permeability of medium, and ω is angular frequency.

2.1.3 Propagation formula for lossy medium

To acquire the RSS for a specific medium for a given distance, the properties of both, the antenna and medium should be considered simultaneously. Assuming that the antennas radiate waves that diverge approximately spherically in the far-field area and propagate with the plane waves in the medium, we can estimate the combined formula for EM waves. Considering the transmission power and properties of the EM waves, we combine the attenuation constant, (2), and the Friis-Shelkunoff formula, (1), to obtain

$$P_R = \frac{P_T G_T G_R \lambda^2}{(4\pi R)^2} e^{-2R\alpha} \text{ [mW]}. \tag{4}$$

The equation above is rearranged and simplified as follows:

$$P_R = \frac{e^{-2\alpha R}}{R^2} \times cm \tag{5}$$

where c is a constant, independent of R. To change the unit to decibel (dB), we take the logarithm of both sides:

$$10\log_{10} P_R = -20\log_{10} R - 20\alpha R \log_{10} e + 10\log_{10} c. \tag{6}$$

By replacing the transfer power $10\log_{10} P_R$, $10\log_{10} P_T$, and $10\log_{10} c$ with new log-scale constant RSS (or S_R), S_T, and C, respectively, the RSS equation with distance can be modeled as follows:

$$RSS = -20\log_{10} R - 20R\alpha \log_{10} e + C \text{ [dBm]}, \tag{7}$$

$$C = 20\log_{10} \frac{\lambda}{4\pi} + 10\log_{10} G_T + S_T + 10\log_{10} G_R + 10\log_{10} PLF + w, \tag{8}$$

where λ is the wavelength of EM waves, PLF is the polarization loss factor, and w is an additional unknown attenuation factor.

As shown in (7), the RSS of underwater EM waves is calculated as the sum of the logarithmic and linear functions of R and the constant term [11, 14].

2.2. Sensor model calibration as parameter estimation

Generally, it is difficult to accurately calculate C and α because each parameter is affected by many environmental conditions (the antenna impedance mismatch caused by the medium, unmodeled environmental effects, noise, etc.) and the medium properties (conductivity, permeability, and permittivity). Moreover, periodic measurements of the sensor parameters is necessary because the EM waves attenuation ratio can vary continuously. However, it is very difficult to periodically check the parameters, and additional equipment is required, further complicating the process. This can be overcome if the localization system has more than three anchor nodes (having specified localizations with known positions), as we can conduct a parameter estimation using the localization system characteristics.

Almost all RSS-based localization systems for use in a structured environment rely heavily on anchor nodes, as shown in Fig. 2. The anchor nodes $(1, 2, \cdots, i, j)$ provide known positions and distances. By substituting our RSS estimates (RSS_{12}, RSS_{13}, $\cdots$, RSS_{ij}) and their known distances (R_{12}, R_{13}, $\cdots$, R_{ij}) into Eq.7, we can estimate the parameters, α and C using input / output mapping as the follows:

$$RSS_{12} = -20\log_{10} R_{12} - 20R_{12}\alpha \log_{10} e + C,$$
$$RSS_{13} = -20\log_{10} R_{13} - 20R_{13}\alpha \log_{10} e + C,$$

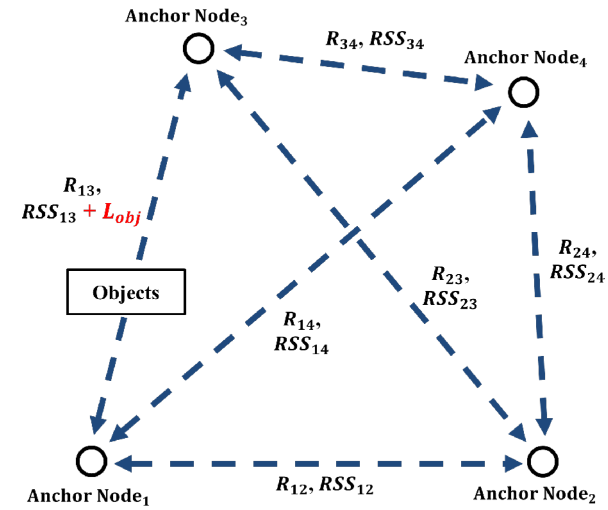

Fig. 2. Conceptual diagram of parameter estimation method using anchor node information. Using the estimated value RSS_n at a reference distance R_n, a user can determine C and α. However, if a structure exists between two anchor nodes, such as anchor node_1 and anchor node_3, it induces parameter estimation uncertainty due to an additional loss (L_{obj}).

$$\vdots$$

$$RSS_{ij} = -20\log_{10} R_{ij} - 20R_{ij}\alpha \log_{10} e + C. \tag{9}$$

Therefore, we can easily approximate α and C using the least squares method. However, if a structure exists between the anchor nodes during parameter estimation, it induces uncertainty. Therefore, open space conditions must be maintained for the sensor network during the calibration scheme.

3. ANALYSIS OF EM WAVES INTERFERENCE NEAR OBJECTS

Generally, propagating EM waves are considered to radiate into an unbounded medium. However, the presence of a structure, especially one near the radiating element, can significantly alter the overall radiation properties of the antenna system. In fact, in most cases, structures exist in the propagation paths of EM waves (even in the absence of any other objects, the ground is present). Therefore, it is important to understand the environmental influence on the EM waves propagation paths.

However, estimation of energy loss due to this interference is difficult. The interference can be classified as penetration, deflection, or diffraction interference, with each being influenced by the object characteristics such as radius, thickness, material properties, and shape. If an EM waves energy loss model incorporating all the characteristics were developed, it would provide a convenient means of estimating the additional attenuation power. However, a model measuring all the characteristics is infeasible and would also generate large computation loads. Moreover, it is difficult to measure the variable factors depending on the mobile node (having random, unknown positions) conditions, such as the incidence angle and surface roughness.

Therefore, it is important to minimize the effects of the objects through EM waves propagation analysis, and to design an additional loss model for significant interferences.

3.1. Fresnel zone in water

EM waves propagation may be interrupted by objects located between the transceivers, causing phase shifting of the EM waves; the effects of phase shifting cannot be measured precisely. As an alternative, the effects of interference can be analyzed using the Fresnel zone, which can analyze interference due to objects near the EM waves paths [20, 21]. The general equation for calculating the Fresnel zone radius F_n follows [22]:

$$F_n = \sqrt{\frac{n\lambda d_1 d_2}{d_1 + d_2}}, \tag{10}$$

where n is the order of Fresnel zone, and d_1, d_2 are the distances between the objects and nodes, as shown in Fig. 3.

The object-induced EM waves interference decreases dramatically as n increases. Therefore, a high-order Fresnel zone must be kept largely free from obstructions to avoid interference with the radio reception. In that case, the EM waves propagation would be minimally affected by the object, and the EM waves could be assumed to propagate in open space. However, if some parts of the Fresnel zone encountered objects, the EM waves could experience the multi-path effect. Estimation of this effect is difficult because of the condition-dependent variables. If the objects occupied the entire Fresnel zone, the EM waves signal would propagate to the receiving antenna through almost complete penetration of objects and uniform signal loss. The underwater Fresnel zone is smaller than that in air, because λ decreases in a denser medium ($\lambda_{water} \approx \lambda_{air}/8.8$, at 420 Mhz, 25°C).

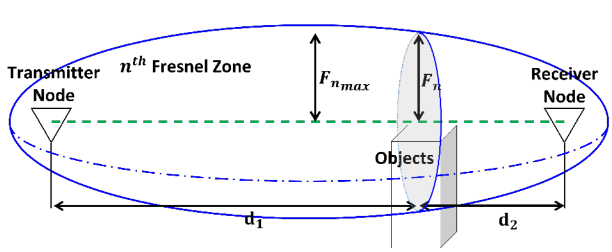

Fig. 3. Conceptual diagram of Fresnel zone. The Fresnel zone is the region of EM waves interference induced by objects located between the transmitter and receiver. $F_{n_{max}}$: maximum Fresnel zone order.

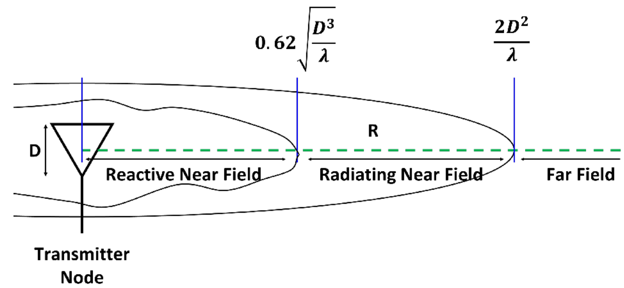

Fig. 4. Conceptual diagram of near-field region. EM waves exhibit an irregular radiation pattern near the transmitter because of the phase gap between E- and H-fields. Although the objects belong to the transmitter near the field, the fields degrade as a function of $1/R$, while the power density degrades as a function of $1/R^2$.

3.2. Near-field region

Another factor influencing the propagation characteristics of EM waves, is the distance from the transmitter (Fig. 4). Near the transmitter, the EM waves radiation pattern does not change shape with distance. In the immediate vicinity of the transmitter, however, the EM waves have a reactive near field, which means the electric (E-) and magnetic (H-) fields are out of phase by 90 degrees relative to each other. The equation for calculating the reactive near field follows [23]:

$$R < 0.62\sqrt{\frac{D^3}{\lambda}}, \tag{11}$$

where D denotes the maximum linear dimension of the antenna.

The radiating near field is the region between the near and far fields. In this region, the reactive fields are not dominant; however, the radiation pattern shape may vary significantly with distance. The equation for calculating the radiating near field is the follows:

$$0.62\sqrt{\frac{D^3}{\lambda}} < R < \frac{2D^2}{\lambda}. \tag{12}$$

Although the objects are positioned in the transmitter near the field, the fields still degrade as a function of $1/R$, while the power density degrades as a function of $1/R^2$.

4. EM WAVES PROPAGATION EXPERIMENTS NEAR OBJECTS

Three experiments were conducted in a water basin to verify the characteristics of EM waves propagation near objects: 1) antenna input impedance measurement near the objects to analyze the near-field effects; 2) RSS measurement near the objects to analyze the EM waves multi-path

Table 1. Experimental environment constants.

	Property (symbol)	Values [unit]
Freshwater	Conductivity (σ)	0.075 [S/m]
	Permeability (μ)	1.2566×10^{-6} [H/m]
	Permittivity (ε)	7.2797×10^{-10} [F/m]
	Wavelength at 420Mhz (λ)	0.0811 [m]
	Refraction index (n)	8.8
Antenna	Antenna gain (G_T, G_R)	3[dBi]
	Input impedance (Z_{in})	$67.132 + j20.263$ [Ω]
	Maximum linear dimension (D)	0.315 [m]
	Transmitting Power (S_T)	10 [dBm]
	Operation frequency (f)	420 [MHz]

effects according to the Fresnel zone; and 3) RSS measurement to analyze the EM waves penetration loss characteristics inside the Fresnel zone.

4.1. Common experimental environment

To analyze the EM waves interference, we performed an experiment in the underwater test facility in the Korea Institute of Robots and Technology Convergence (KIRO). The test tank was 12 m long, 8 m wide, and 6 m deep. To prevent EM waves reflection, the antennas were separated from the wall by 1.5 m using an aluminum experimental guide rail, and were submerged 1.5 m in depth. Half-wavelength sleeve-dipole antennas, with an antenna gain of 3 dBi were used, and transmitting and receiving antennas were installed (Table 1). To ensure proper alignment between the antennas, antenna frames were employed. The distance between the antennas was measured as the distance between the antenna frames using a tapeline and a laser range finder. The medium inside the basin was assumed to be fresh water. EM waves generation and signal reception were performed using a National Instruments signal generator (NI5660SA) and signal analyzer (NI5670SG). The transmitting power was set to 10 mW (10 dBm) with 420 MHz frequency.

4.2. Input impedance influence near objects

4.2.1 Conditions and procedure

The experimental environment was configured to analyze the input impedance influence in the vicinity of objects, as shown in Fig. 5. A network analyzer (Agilent Technologies N5230A) measured the input impedance of the transmitter antenna at 420Mhz according to the distance (height) between the transmitter and object. The height difference between the antenna and object incrementally increased by 0.01 m from 0.03 m to 0.5 m. A steel and wood plate (dielectric constant ≈ 2) were used to analyze the effects of an object.

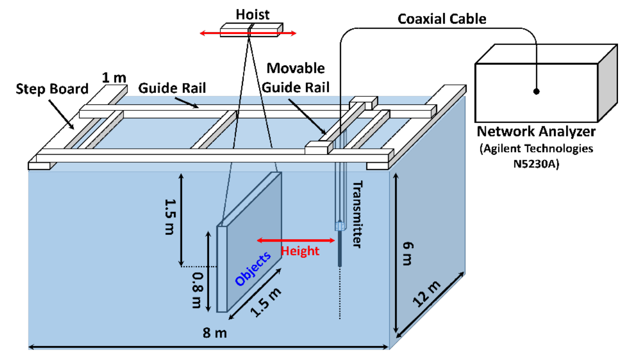

Fig. 5. Schematic diagram of input impedance experiment near objects.

4.2.2 Results

The input impedance versus distance was recorded, Fig. 6. The input impedance value apparently increased when the height was less than 2 λ. However, when the distance between the antenna and object exceeded 2 λ and D, the input impedance value was similar to that in an open environment, despite it being associated with the reactive near field. Hence, it was estimated that water has different near-field characteristics compared to air because it is a lossy medium. Based on this experiment, it is recommended that a minimum distance from the structures of D and 2 λ be maintained during transmitter installation, to prevent antenna impedance mismatching and the near-field effect.

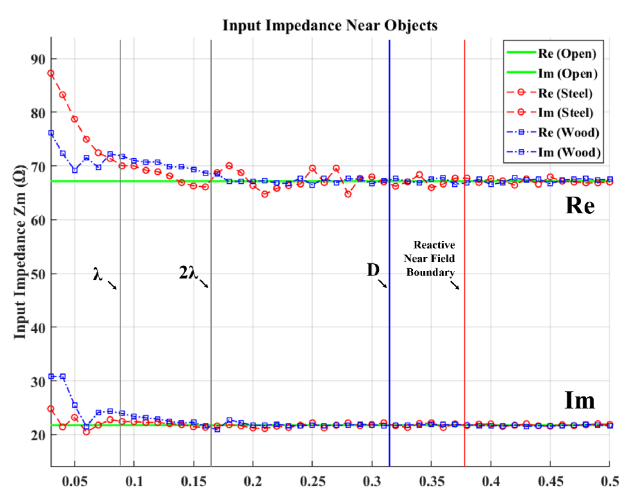

Fig. 6. Input impedance versus height. When the distance between the antenna and object exceeded 2 λ and D, the input impedance value was similar to that in an open environment despite it being associated with the reactive near field.

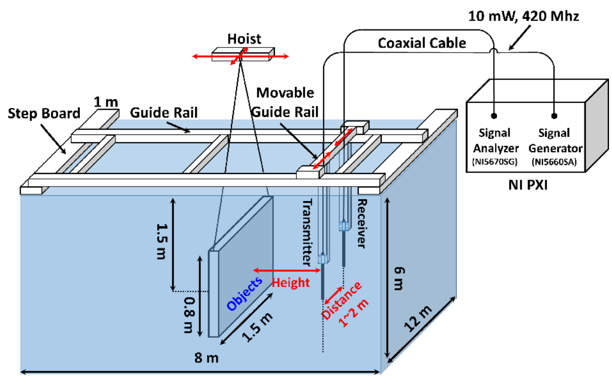

Fig. 7. Schematic diagram of EM waves interference experiment in Fresnel zone. Where distance is the gap between transceivers, and height is gap between transceiver and object.

4.3. EM waves interference in Fresnel zone

4.3.1 Conditions and Procedure

The experimental environment was configured to analyze the EM waves interference in the Fresnel zone, as shown in Fig. 7. The signal analyzer measured the RSS of the EM waves at 420 Mhz, according to distance and height. The height difference between the antenna and object incrementally increased by 0.025 m, from 0.1 to 0.55 m. This experiment was repeated three times with changes in the distance between the transmitter and receiver ($R = 1$, 1.5, and 2 m). A steel and wood plate were used to analyze the object effects.

4.3.2 Results

The RSS values versus height (distance) were collected; results are shown in Fig. 8. As the distance between the antennas and the object increased, the RSS value converged to that obtained in the open environment. The change in RSS value became more prominent as the distance between the two antennas increased because the radius of the Fresnel zone also increased. The RSS values exhibited large unexpected fluctuations with considerable standard derivations when the objects were positioned in the 1st and 2nd Fresnel zones. Hence, the multi-path effects of the EM waves were estimated. However, there were a few RSS changes when the height exceeded the radius of the 4th Fresnel zone. Based on this experiment, we recommended that a minimum distance (height) equivalent to the radius of the 4th Fresnel zone is maintained between the antennas and structures, to prevent unexpected RSS changes due to the multi-path effect.

4.4. Penetration loss by objects

4.4.1 Conditions and Procedure

The experimental environment was configured to analyze the EM waves interference when the entire 4th Fres-

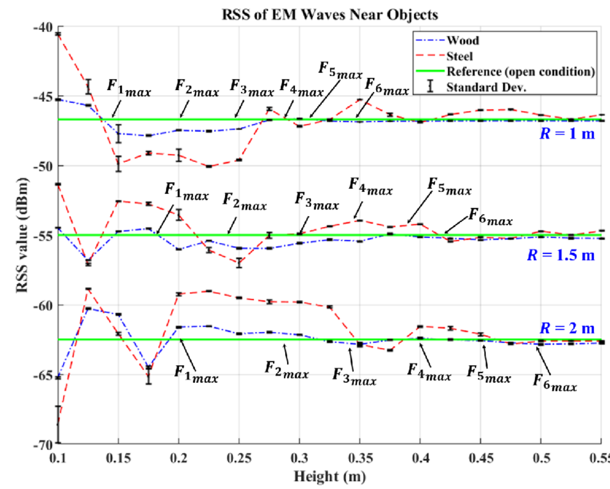

Fig. 8. EM waves RSS versus height and distance. This figure shows that the additional loss due to the object penetration exhibited specific and uniform attenuation regardless of the antenna distance and object position, when the object occupied the entire 4th Fresnel zone.

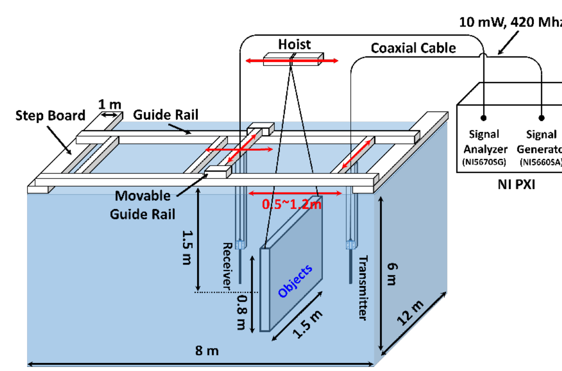

Fig. 9. Schematic diagram of experiments for EM waves penetration effect in Fresnel zone.

nel zone was occupied by objects, as shown in Fig. 9. The signal analyzer measured the RSS of the EM waves at 420 Mhz in two experiments considering (1) changes to the relative position between the object and antennas in the EM wave propagation direction (Fig. 10(a)) and (2) changes to the distance between the antennas, with a fixed object position (Fig. 10(b)).

4.4.2 Results

The two experimental setups and corresponding experimental results are shown in Fig. 10; the additional power attenuation due to penetration has an almost constant value regardless of the antenna position, distance, and relative object position.

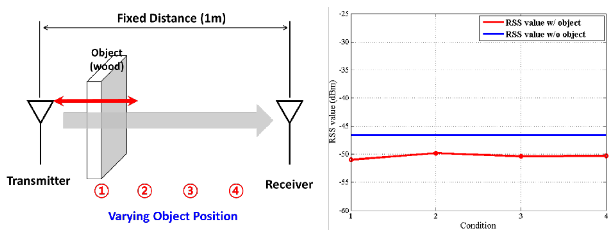

(a) Case 1: Fixed overall distance with varying relative position between object and antennas (in propagation direction).

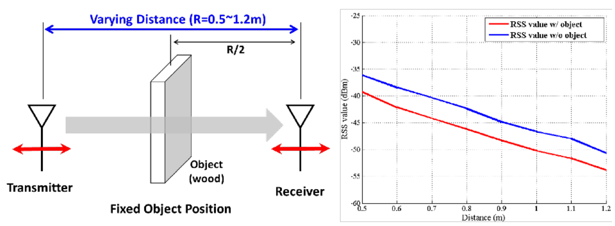

(b) Case 2: Fixed relative object position with varying distance between antennas.

Fig. 10. Experiment results for additional EM waves attenuation due to penetration effect. Each result indicates additional EM waves attenuation due to penetration which has a constant value regardless of object position and distance between antennas.

4.5. Conclusion regarding underwater EM waves interference near objects

Underwater EM waves interference near objects showed different characteristics compared to air. In particular, the input impedance value was similar to that obtained in an open environment, despite being associated with the reactive near field. Furthermore, the RSS of the EM waves indicated that a few multi-path effects occurred when the gap between the propagation line and object exceeded the radius of the 4th Fresnel zone. This behavior occurred because a water medium has a short wavelength compared to an air medium at the same frequency, and the former is regarded as a lossy medium. Note, the multi-path effects disappeared because of the large signal attenuation along the additional travel distance. Also, additional loss due to the object penetration exhibited specific and uniform attenuation, regardless of the antenna distance and object position when the object occupied the entire 4th Fresnel zone. Therefore, the penetration loss model, along with the object characteristics, are incorporated in the proposed EM waves distance-attenuation model for structured environments.

5. DERIVATION OF UNDERWATER RANGE SENSOR MODEL FOR STRUCTURED ENVIRONMENTS

5.1. EM waves penetration loss model

When an object is positioned between the transmitter

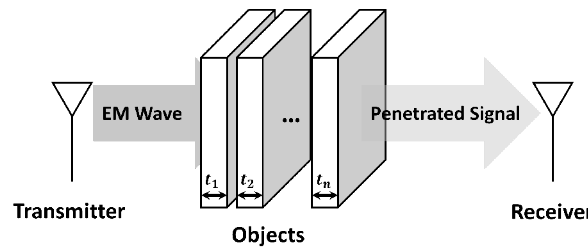

Fig. 11. Influence factors of EM waves attenuation when EM waves penetrate objects. The penetration attenuation is affected by the object depth and material type.

and receiver antennas, with the entire 4th Fresnel zone occupied by the object, we can assume that EM waves experience additional loss due to penetration. This penetration loss can be expressed by an equation with object depth and object number, as shown below in Fig. 11 [24, 25]:

$$L_{obj} = \beta n + \gamma t_m \text{ [dB]}. \tag{13}$$

L_{obj} is intended to capture the additional attenuation due to object, n, with total object thickness $t_m = t_1 + t_2 + \cdots + t_n$, located between the transmitter and receiver. The first calibration factor, β, is given in dB per object and represents the additional attenuation caused by penetration. The second calibration factor, γ, is given in dB per meter and represents the attenuation factor due to the material.

In addition to the penetration loss model, which only considers penetration relative to the underwater sensor model for EM waves attenuation, the sensor model can estimate the transmitter-receiver separation robustly in a structure-containing environment. Subtracting (13) from (7), the following model is obtained:

$$RSS = -20\log_{10} R - 20R\alpha \log_{10} e + C - \beta n - \gamma t_m. \tag{14}$$

5.2. Calibration factor experiments

Two experiments were performed to develop and verify the improved underwater sensor model. The RSS values in various structure materials were measured to determine β and γ according to the material as shown in Fig. 13. The calibration factors were determined based on the object materials. Because most underwater structures and facilities consist of stone, wood, or steel, the calibration factor experiments were conducted using those materials.

5.2.1 Conditions and procedure

A model of the experimental environment is presented in Fig. 13. The objects were 1.5 m wide and 0.8 m long, with varying thickness. The objects were deployed between the antennas, hanging from two hoists. The distance between the nodes was 1 m.

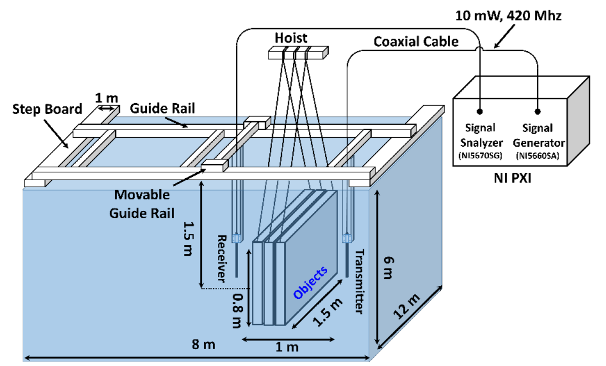

Fig. 12. Schematic diagram of setup for material calibration factor experiments.

Table 2. Calibration factor experiment conditions.

	n	t_m [m]	L_{obj}		n	t_m [m]	L_{obj}
Wood	1	0.015	2.0906	Stone	1	0.02	2.9960
	1	0.024	2.9292		1	0.03	3.4173
	2	0.030	4.0958		2	0.04	6.5826
	2	0.039	5.1298		2	0.05	6.9262
	2	0.048	5.9621		2	0.06	7.3574
Acrylic	1	0.002	1.3217	Steel	1	0.002	43.4537
	1	0.005	2.3662				
	2	0.007	5.7280		2	0.007	43.5414
	2	0.010	6.8202				

First, the RSS values without the object, $S_{w/o}$, were measured. The experiments were then repeated for varying object thickness, yielding $S_{w/}$. Materials used were wood, stone, and steel. When n exceeded 1, the gap between objects was kept at 5 mm using support. L_{obj} was determined by subtracting $S_{w/}$ from $S_{w/o}$. Finally, β and γ values were calculated using the least squares method. The experiment conditions are listed in Table 3.

5.3. Experiment results

The calibration factors according to the materials are presented in Table 3. In the case of dielectric materials such as stone and wood, L_{obj} linearly increased depending on the object t_m and n. EM waves cannot penetrate steel because of its conductivity; therefore, L_{still} had the largest value despite the small object thickness. Thus, L_{still} can be considered as another distortion effect, similar to diffraction and reflection. Note, the effects of the other distortions were trivial.

Table 3. Experiment result for calibration factors.

	β [dB/n]	γ [dB/m]
Wood	0.6332	96.3408
Stone	2.3101	45.1200
Acrylic	1.4211	35.7411

6. LOCALIZATION EXPERIMENT IN ENVIRONMENT WITH UNDERWATER STRUCTURES

A 2D localization experiment in an infrastructure-based localization system was performed to verify the performance for a structured environment.

6.1. Experimental conditions and procedure

To analyze the penetration model performance, mobile node localization was conducted in an object-containing environment. The experimental environment consisted of three anchor nodes, and three mobile nodes, with a 2.54-m-long and 2.54-m-wide square test bed, as shown in Fig. 14. The anchor nodes were fixed near the edge of the test bed with known positions. The mobile nodes were located on the inner area of the test bed and received signals from the anchor nodes. The object hung on the hoists, positioned approximately perpendicular to the mobile nodes. To analyze the node localization performance, all nodes were measured using a laser distance-measuring instrument. It was assumed the EM waves signal weakened as a result of object penetration only, and the object thickness and material were known.

To verify the sensor model performance for the non-object environment, mobile nodes were estimated. The anchor nodes transmitted EM waves with various frequency bands, and the mobile nodes identified each anchor node. Nodes 1 and 2 received signals from the anchor nodes, and estimated the distance using the sensor model; each node then estimated its position. Next, to verify the sensor model performance for a structure-containing environment, the position of mobile node 3 was estimated. Mo-

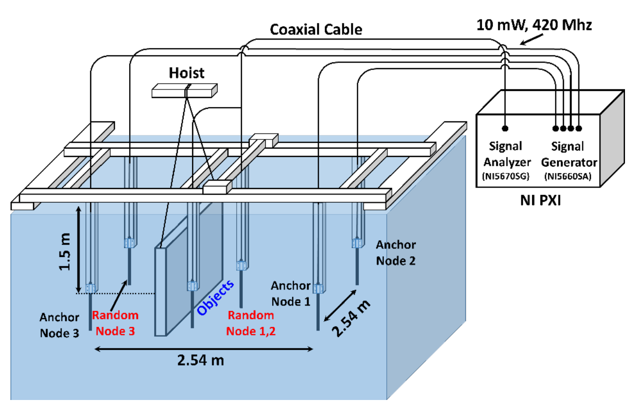

Fig. 13. Schematic diagram of localization environment with structure. Anchor nodes were fixed near the edge of the test bed. Mobile nodes 1 and 2 estimated their positions using the received signal; then, transmitted signals with their own frequency. Mobile node 3 estimated its position using the penetrated signal.

Table 4. Mobile node localization conditions and results.

Dimension [m]							
	Mobile node 1	Mobile node 2	Mobile node 3				
			Mobile node 3 (Wood)		Mobile node 3 (Steel)		
			w/o model	w/ model	w/o model	w/ model	
Actual position	[1.0200, 1.4700]	[1.2700, 1.2700]	[2.5400, 2.5400]				
Estimated position	[1.0194, 1.4693]	[1.2698, 1.2696]	[2.7136, 2.6799]	[2.5585, 2.5629]	[2.6949, 2.6579]	[2.5619, 2.5568]	
Maximum error	0.0038	0.0020	0.2262	0.0322	0.1980	0.0311	
Minimum error	0.0003	0.0001	0.2194	0.0276	0.1913	0.0244	
RMS error	0.0014	0.0008	0.2230	0.0296	0.1947	0.0277	

bile nodes 1 and 2 broadcast their own estimated positions on different frequency bands. Mobile node 3 received the signals from the two mobile nodes, and then estimated its own position. In order to analyze the penetration loss model performance, a different sensor model was used. That is, one sensor model had no additional loss factor for objects, while the other incorporated an additional loss factor.

6.2. Localization result

The localization results are shown in Figs. 14 and 15. The localization results of mobile nodes 1 and 2 are shown in Figs. 15(a) and 15(b). These figures show good position estimation results, and the estimated positions were inside the covariance ellipse with insignificant error. Therefore, good localization performance was achieved for non-object environments. The localization performance according to the structure material is shown in Figs. 15(c) (stone) and 15(d) (wood). Regardless of the penetration model, there were gaps between the localization results and the actual positions. This may have been caused by additional distortion of the EM waves or environmental effects. However, the performance of the sensor with the penetration loss model significantly improved without the penetration loss model. As described in Table. 4, the RMS errors decreased by 90%.

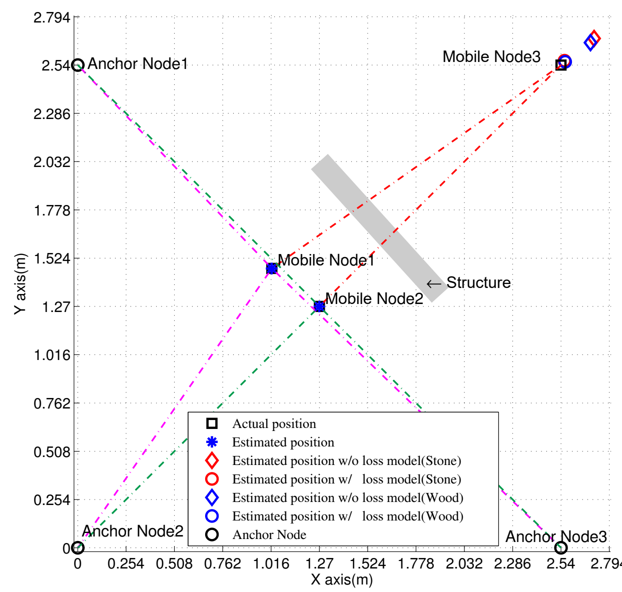

Fig. 14. Mobile node localization conditions and results.

7. CONCLUSION

In this study, the characteristics of EM waves propagation in a structured underwater environment were analyzed to identify the signal interference caused by the structure, and an EM waves attenuation model considering the distance and penetration loss induced by the structure was suggested.

The near-field and multi-path effects in the Fresnel zone were considered as influencing factors of EM waves propagation characteristics. The results of several experiments indicated that the underwater EM waves interference near objects exhibit different characteristics to that encountered in air. In particular, the input impedance value was similar to the input impedance in an open environment, despite it corresponding to the reactive near field. Further, the RSS of the EM waves exhibited few multi-path effects when the gap between the propagation line and object exceeded the radius of the 4th Fresnel zone. Furthermore, the additional loss due to the object penetration showed specific and uniform attenuation characteristics, regardless of antenna distance and relative object position, when the entire 4th Fresnel zone was occupied by the object.

Based on the EM waves propagation analysis, the object penetration loss was incorporated into the EM waves additional loss model for application in structured underwater environments. The proposed penetration loss model showed consistent and repeatable attenuation estimation capabilities. Underwater localization in the structured environment was conducted using the proposed sensor model, and improved position estimations result with low bias error were obtained. These results indicate that it is expected to be used for localization in structured environments such as autonomous docking and inspections of the facilities.

In the future, we will conduct additional experiments

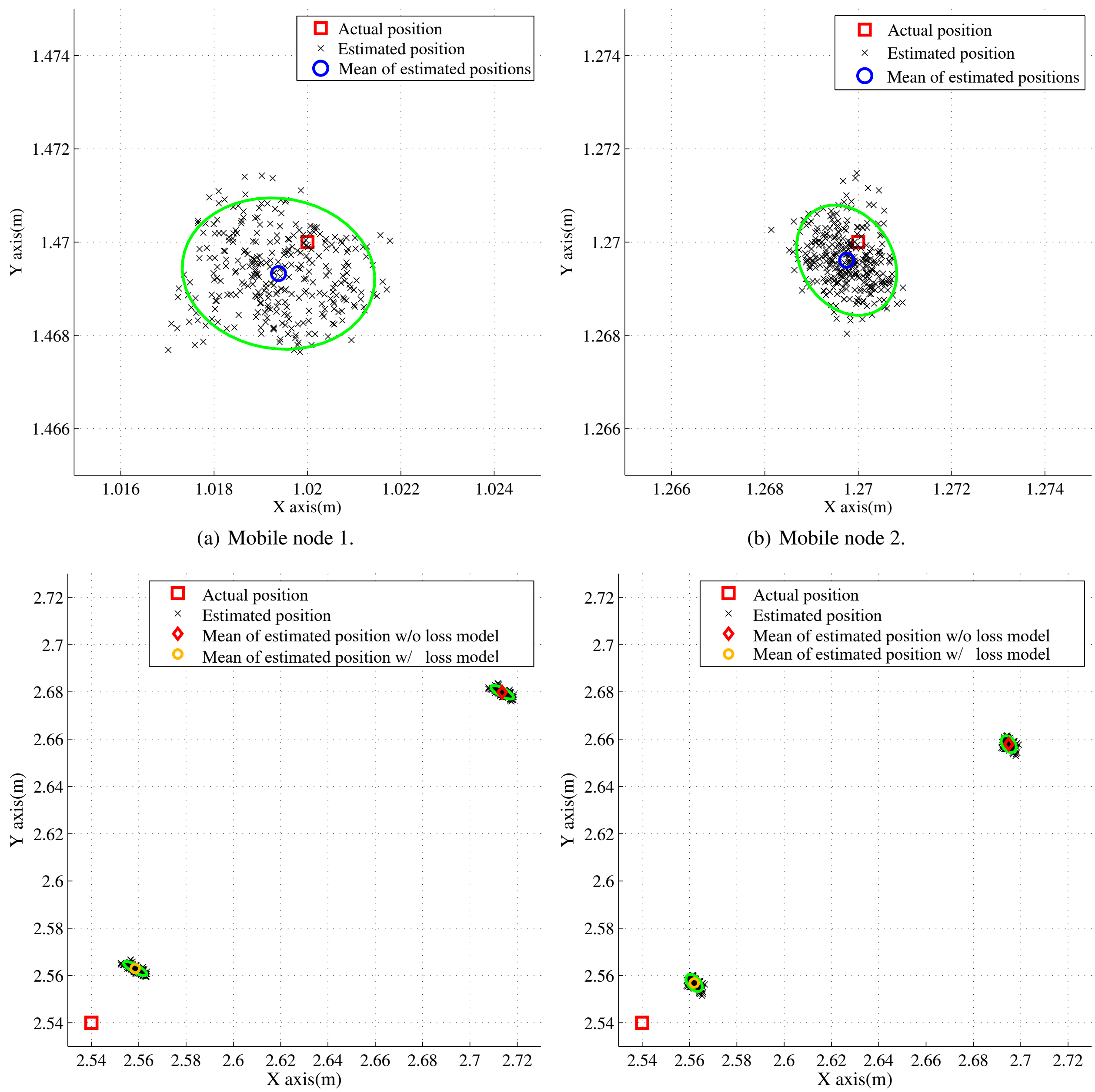

(a) Mobile node 1.

(b) Mobile node 2.

(c) Mobile node 3 with structure (Stone).

(d) Mobile node 3 with structure (Wood).

Fig. 15. Mobile node localization results.

involving various materials and conditions (e.g., real sea conditions), and will determine the relationship between the EM waves propagation and object interference. In addition, we will apply several algorithms and sensors to improve the localization range and accuracy.

REFERENCES

[1] L. Paull, S. Saeedi. M. Seto, and H. Li, "AUV navigation and localization: a review," *IEEE Journal of Oceanic Engineering*, vol. 39, no. 1, pp. 131-149, 2014.

[2] G. Marani and S. Choi, "Underwater target localization," *IEEE Robotics & Automation Magazine*, vol. 17, no. 1, pp. 64-70, 2010.

[3] M. Sualeh and G.-W. Kim, "Simultaneous localization and mapping in the epoch of semantics: a survey," *International Journal of Control, Automation and Systems*, vol. 17, no. 3, pp. 729-742, 2019.

[4] G. Tuna and V. C. Gungor, "A survey on deployment techniques, localization algorithms, and research challenges for underwater acoustic sensor networks," *International Journal of Communication Systems*, vol. 30, no. 17, e3350, 2017.

[5] J. H. Li, M. J. Lee, J. G. Kim, S. K. Park, S. H. Park, and J. H. Suh, "Guidance and control of P-SURO II hybrid AUV," *Proc. of the IEEE OCEANS*, pp. 1-7, 2012.

[6] I. Akyildiz, D. Pompili, and T. Melodia, "Underwater acoustic sensor networks: research challenges," *Ad Hoc Networks*, vol. 3, no. 3, pp. 257-279, 2005.

[7] J. Gordon and A. Moscrop, "Underwater noise pollution and its significance for whales and dolphins," *The Conservation of Whales and Dolphins: Science and Practice*, John Wiley & Sons, 1996.

[8] S. Y. Shin, J. I. Namgung, and S. H. Park, "SBMAC: smart blocking MAC mechanism for variable UW-ASN (underwater acoustic sensor network) environment," *Sensors*, vol. 10, no. 1, pp. 501-525, 2010.

[9] S. Park and S. Yi, "Least-square matching for mobile robot SLAM based on line-segment model," *International Journal of Control, Automation and Systems*, vol. 17, no. 11, pp. 2961-2968, 2019.

[10] T. Kim, J. Kim, and S.-W. Byun, "A comparison of nonlinear filter algorithms for terrain-referenced underwater navigation," *International Journal of Control, Automation and Systems*, vol. 16, no. 6, pp. 2977-2989, 2018.

[11] D. Park, K. Kwak, W. K. Chung, and J. Kim, "Development of underwater short-range sensor using electromagnetic wave attenuation," *IEEE Journal of Oceanic Engineering*, vol. 41, no. 2, pp. 318-325, 2016.

[12] D. Park, K. Kwak, J. Kim, and W. K. Chung, "3D underwater localization scheme using EM wave attenuation with a depth sensor," *Proc. of the 2016 IEEE International Conference on Robotics and Automation (ICRA)*, pp. 2631-2636, 2016.

[13] D. Park, K. Kwak, J. Kim, and W. K. Chung, "Received signal strength of electromagnetic waves aided integrated inertial navigation system for underwater vehicle," *Proc. of the 2018 IEEE/RSJ International Conference on Intelligent Robots and Systems (IROS)*, pp. 1870-1876, 2018.

[14] D. Park, K. Kwak, W. K. Chung, and J. Kim, "Development of underwater distance sensor using EM wave attenuation," *Proc. of the 2013 IEEE International Conference on Robotics and Automation (ICRA)*, pp. 5125-5130, 2013.

[15] A. I. Al-Shamma, A. Shaw, and S. Saman, "Propagation of electromagnetic waves at MHz frequencies through seawater," *IEEE Transactions on Antennas and Propagation*, vol. 52, no. 11, pp. 2843-2849, 2004.

[16] U. Qureshi, F. Shaikh, Z. Aziz, S. Shah, A. Sheikh, E. Felemban, and S. Qaisar, "RF path and absorption loss estimation for underwater wireless sensor networks in different water environments," *Sensors*, vol. 16, no. 6, pp. 1-15, 2016.

[17] D. Park, K. Kwak, W. K. Chung, and J. Kim, "Infrastructure-based localization system using underwater wireless sensor network," *Journal of Institute of Control, Robotics and System*, pp. 699-705, 2012.

[18] H. T. Friis, "Introduction to radio and radio antennas," *IEEE Spectrum*, vol. 8, no. 4, pp. 55-61, 1971.

[19] F. T. Ulaby, U. Ravaioli, and E. Michielssen, *Fundamentals of Applied Electromagnetics*, Prentice Hall, 2014.

[20] B. Barshan and R. Kuc, "Differentiating sonar reflections from corners and planes by employing an intelligent sensor," *IEEE Trans. on Pattern Analysis and Machine Intelligence*, vol. 12, no. 6, pp. 560-569, June 1990.

[21] V. U. Zavorotny and A. G. Voronovich, "Scattering of GPS signals from the ocean with wind remote sensing application," *IEEE Trans. on Geoscience and Remote Sensing*, vol. 38, no. 2, pp. 951-964, March 2000.

[22] R. L. Freeman, *Radio System Design for Telecommunication*, John Wiley & Sons, 2006.

[23] C. Balanis, *Antenna Theory Analysis and Design*, John Wiley & Sons, 2005.

[24] S. Ahmed, G. C. Karmakar, and J. Kamruzzaman, "An environment-aware mobility model for wireless ad hoc network," *Computer Networks*, vol. 54, no. 9, pp. 1470-1489, 2010.

[25] C. Sommer, D. Eckhoff, R. German, and F. Dressler, "A computationally inexpensive empirical model of IEEE 802.11 p radio shadowing in urban environments," *Proc. of 8th International Conference on Wireless On-Demand Network Systems and Services (WONS)*, pp. 84-90, 2011.

Daegil Park received his B.S. degree in mechanical engineering from Seoul National University of Science and Technology, Seoul, Korea, in 2011, and an M.S. and a Ph.D. degrees in mechanical engineering from Pohang University of Science and Technology, Pohang, Korea, in 2016. He is a senior researcher in Autonomous Systems Research Center, Korea Institute of Robot and Technology Convergence, Pohang, Korea. His current research interests include the areas of autonomous vehicle, underwater robot, path planning, navigation, sensor, and localization.

Wan Kyun Chung received his B.S. degree in mechanical design from Seoul National University, Seoul, Korea, in 1981 and an M.S. degree in mechanical engineering, and a Ph.D. in production engineering from Korea Advanced Institute of Science and Technology (KAIST), Daejeon, Korea, in 1983 and 1987, respectively. He is a Professor in the School of Mechanical Engineering, Pohang University of Science & Technology (POSTECH), Pohang, Korea (he joined the faculty in 1987). In 1988, he was a Visiting Professor at the Robotics Institute, Carnegie Mellon University, Pittsburgh, PA, USA. In 1995, he was a Visiting Scholar at the University of California Berkeley, Berkeley, CA, USA. His research interests include development of robust controllers for precision motion control, biomedical robotics and underwater robots. He served as senior editor for IEEE TRO and regional editor for Journal of Intelligent service robotics.

Jinhyun Kim received his B.S., M.S., and Ph.D. degrees in mechanical engineering from Pohang University of Science and Technology, Pohang, Korea, in 1998, 2000, and 2005, respectively. In 2007, he joined Seoul National University of Science and Technology, Seoul, Korea, where he is currently a Professor with the School of Mechanical Engineering. His current research interests include the areas of redundant manipulators, underwater robots, hovering robots, and neuro-robotics.